Title	State-of-the-art review on low-velocity impact response of reinforced concrete beams
Author(s)	Adhikary, Satadru Das; Li, Bing; Fujikake, Kazunori
Citation	Adhikary, S. D., Li, B., & Fujikake, K. (2016). State-of-the-art review on low-velocity impact response of reinforced concrete beams. Magazine of Concrete Research, 68(14), 701-723.
Date	2016
URL	http://hdl.handle.net/10220/42706
Rights	© 2016 ICE Publishing. This paper was published in Magazine of Concrete Research and is made available as an electronic reprint (preprint) with permission of ICE Publishing. The published version is available at: [http://dx.doi.org/10.1680/jmacr.15.00084]. One print or electronic copy may be made for personal use only. Systematic or multiple reproduction, distribution to multiple locations via electronic or other means, duplication of any material in this paper for a fee or for commercial purposes, or modification of the content of the paper is prohibited and is subject to penalties under law.

Magazine of Concrete Research
Volume 68 Issue 14

State-of-the-art review on low-velocity impact response of reinforced concrete beams
Adhikary, Li and Fujikake

Magazine of Concrete Research, 2016, **68**(14), 701–723
http://dx.doi.org/10.1680/jmacr.15.00084
Paper 1500084
Received 17/02/2015; revised 27/09/2015; accepted 15/10/2015
Published online ahead of print 27/11/2015
Keywords: beam & girders/concrete structures/dynamics

ice
Institution of Civil Engineers
publishing

State-of-the-art review on low-velocity impact response of reinforced concrete beams

Satadru Das Adhikary
Research Fellow, Department of Civil and Environmental Engineering, National University of Singapore, Singapore
(corresponding author: 2020satadru@gmail.com)

Bing Li
Associate Professor, School of Civil and Environmental Engineering, Nanyang Technological University, Singapore

Kazunori Fujikake
Professor, Department of Civil and Environmental Engineering, National Defense Academy, Yokosuka, Japan

Based on a comprehensive literature review, a state-of-the-art report on the strain rate dependent mechanical properties of materials involved in reinforced concrete (RC) structures and the structural response of RC beams under low-velocity impact is presented. Due to the prevalence of plentiful equations to calculate the dynamic increase factor of concrete strength in compression and tension, future research is needed to reach a general consensus. Two empirical equations were derived based on previous test data, and the applicability of the proposed equations is demonstrated. With the interpretation of previous data in the light of authors' test results, the issue related to a change in failure mode from flexural failure under static loading to shear failure under impact loading is discussed. Finally, several issues related to the impact response of beams are raised, and the need for future research is identified.

Notation

a	shear span of beam
b	width of beam
d	effective depth of beam
E	input impact energy
f'_c	compressive strength of concrete
f_{Ly}	yield strength of longitudinal reinforcements
f_{Ty}	yield strength of transverse reinforcements
h	total height of beam
L	total length of beam
R_b	bending resistance of RC beam
R_s	shear resistance of RC beam
δ_{max}	maximum midspan deflection

Introduction

It is generally admitted that there is an apparent increase in strength when a concrete-like material is subjected to a high strain rate. The dynamic increase factor (DIF), defined as the ratio of dynamic strength to quasi-static strength, is widely accepted as an important parameter in the measurement of strain rate dependent material behaviour. However, there are several hypotheses concerning the physical mechanism explaining the concrete material response under varying strain rates. One of them states that the observed strain rate effect is due to the presence of water, which may influence the response of concrete under high strain rates (Rossi *et al.*, 1994). It is known that the Stefan effect on free water within concrete can change the cracking patterns under high loading rates. Under quasi-static loading, cracks occur in the cement matrix, and when these cracks encounter coarse aggregates they propagate around the boundaries of the aggregate. On the other hand, in dynamic loading, due to the Stefan effect, cracks would penetrate through the coarse aggregates and this may be the reason behind the strength enhancement.

Another perspective is the lateral inertia force effect, which causes an apparent increase in the DIF of concrete. Li and Meng (2003) reported that an increase in dynamic compressive strength could only be caused by lateral confinement when the strain rate is higher than around 100 s^{-1}. They termed this lateral inertia confinement 'the pseudo strain rate effect' and further opined that acceptance of this strain rate effect in design and numerical models may overestimate the dynamic compressive strength of concrete. On the other hand, Zhou and Hao (2008) developed a homogeneous meso-scale model with a strain rate sensitive material model to analyse concrete-like material under high strain rate compression, and the model was found to corroborate reasonably well with test results.

Comparison of the DIF caused by lateral confinement and the DIF obtained from dynamic tests shows that inertial confinement is only one of the two sources that contribute to the DIF,

and this contribution becomes more significant when the strain rate is higher than 1000 s^{-1}. Material strain rate effects cannot be neglected in modelling the concrete material response to high loading rates, especially when the strain rate is less than 200 s^{-1}.

Kim *et al*. (2010) performed numerical simulations on concrete specimens under high strain rates in compression to see whether the experimentally (i.e. split Hopkinson pressure bar (SHPB) test) obtained strain rate effects were a purely material response or not. It was concluded that a strain rate dependent model should not be employed in numerical simulation as strain rate effects already account for the effects of lateral confinement. Their simulation results also showed the effects of friction on observed strain rate effects when the aspect ratio of specimens was considered. Furthermore, for future experimental and simulation-based research, they suggested examining the specific contribution of the confinement effect. Cotsovos and Pavlovic (2008) raised the question of the usage of strain rate dependent mechanical properties of concrete under high rates of uniaxial tensile loading, as they concluded they were structural rather than material effects. Lu and Li (2011) performed numerical simulations of direct dynamic tensile, dynamic splitting and spalling tests based on a strain rate independent constitutive model of concrete to check whether the tensile DIF is attributed to strain rate effects or structural effects. It was concluded that the strain rate enhancement of tensile strength is purely a material effect rather than a structural effect at macroscopic level. However, at the micro-level, the strain rate dependent tensile strength increment can be attributed to the inertia effects of microcracks.

More recently, Ozbolt *et al*. (2013) performed numerical studies of compact tension specimens loaded to varying rates. After validating the numerical results with experimental results they commented that, for strain rates lower than approximately 50 s^{-1}, the structural response is controlled by a strain rate dependent constitutive law. However, for higher strain rates, crack branching and a progressive increase in resistance were observed. This was attributed to the effect of structural inertia and not the rate dependent strength of concrete. From a numerical point of view, assuming micro- and meso-scale analysis, the effects of the rate dependency of growing microcracks (e.g. the influence of inertia at microcrack level) and the viscous behaviour of the bulk material between the cracks (e.g. viscosity due to water content) can be accounted for by the constitutive law, whereas the structural inertia effect would be automatically accounted for through dynamic analysis (Ozbolt *et al*., 2011).

This paper is organised as follows. First, an overview of the strain rate effect on concrete mechanical properties (compression and tension) and steel reinforcement behaviour (yield and ultimate stress) is presented. This is followed by an assessment of the structural response of reinforced concrete (RC) beams subjected to low-velocity impact (<10 m/s) at midspan through the assembly of a database from the literature. Limited data were used by Kishi and Mikami (2012) to propose empirical formulae for designing beams (e.g. only statically flexure-critical) under impact loading. This limitation is overcome by compiling data from different researchers, and successively similar empirical formulae are presented for both statically shear-critical and flexure-critical beams under low-velocity impact loading. Finally, some issues related to the failure modes of beams under impact loading are discussed, and the need for future research is identified.

The strain rate effect on mechanical properties of materials

Since the mechanical properties of plain concrete and steel are strain rate dependent, the behaviour of structural members under impact loading conditions can only be accurately predicted by considering the strain rate dependent properties of materials. Therefore, to evaluate structural performance in terms of resistance and behaviour, the constitutive properties of concrete and steel over a wide range of strain rates are required.

Plain concrete

The DIF is often used to characterise the rate sensitivity behaviour of material and the strain rate effect on compression and tension of concrete is typically reported as the DIF (i.e. ratio of dynamic strength to static strength).

Compression

CEB model code 1990 (CEB, 1993) gives the DIF for compressive strength as

$$1.\quad \mathrm{DIF} = \begin{cases} (\dot{\varepsilon}/\dot{\varepsilon}_s)^{1{\cdot}026\alpha_s} & \text{for } \dot{\varepsilon} \le 30\ s^{-1} \\ \gamma_s(\dot{\varepsilon}/\dot{\varepsilon}_s) & \text{for } \dot{\varepsilon}_s > 30\ s^{-1} \end{cases}$$

where $\dot{\varepsilon}$ is the strain rate in the range of 30×10^{-6} s^{-1} to 300 s^{-1}, $\dot{\varepsilon}_s = 30 \times 10^{-6}$ s^{-1} is the static strain rate and $\log \gamma_s = 6{\cdot}156\alpha_s - 2$, in which $\alpha_s = 1/(5 + 9\ f_{cs}/f_{co})$ where $f_{co} = 10$ MPa and f_{cs} is the static compressive strength of concrete.

Soroushian *et al*. (1986) proposed an equation for the DIF of concrete in compression by compiling test results reported by different researchers. This DIF is

$$2.\quad \mathrm{DIF} = 1{\cdot}48 + 0{\cdot}160 \log_{10} \dot{\varepsilon} + 0{\cdot}0127 (\log_{10} \dot{\varepsilon})^2$$

where $\dot{\varepsilon}$ is a strain rate greater than 10^{-5} s^{-1}. However, after observing the wide spectrum of test data, the authors tried to figure out the main source of scatter and noted that the moisture content of concrete is the reason for the variability in results. It was concluded that the strain rate effect on

increasing the compressive strength of concrete becomes more significant as the concrete moisture content increases. The available test data did not show any considerable influence of strain rate on the static compressive strength of concrete. Furthermore, the effect of strain rate on concrete compressive strength was found to be independent of the age of the specimens if their moisture contents were identical. DIFs for dry and wet concrete were suggested as follows.

For dry concrete

$$\text{DIF} = 1{\cdot}48 + 0{\cdot}206\log_{10}\dot{\varepsilon} + 0{\cdot}0221(\log_{10}\dot{\varepsilon})^2 \quad (3)$$

and for wet concrete

$$\text{DIF} = 2{\cdot}54 + 0{\cdot}580\ \log_{10}\dot{\varepsilon} + 0{\cdot}0543\ (\log_{10}\dot{\varepsilon})^2 \quad (4)$$

Ross *et al*. (1995, 1996) and Tedesco and Ross (1998) conducted a series of SHPB tests to investigate the effect of strain rate and moisture content on concrete strength. The DIF equations for compression suggested by Tedesco and Ross (1998) are

$$\text{DIF} = 0{\cdot}00965\log_{10}\dot{\varepsilon} + 1{\cdot}058 \geq 1{\cdot}0 \quad \text{for } \dot{\varepsilon} \leq 63{\cdot}1\ \text{s}^{-1} \quad (5)$$

$$\text{DIF} = 0{\cdot}758\log_{10}\dot{\varepsilon} - 0{\cdot}289 \leq 2{\cdot}5 \quad \text{for } \dot{\varepsilon} > 63{\cdot}1\ \text{s}^{-1} \quad (6)$$

An experimental examination of the dynamic behaviour of concrete and mortar at very high strain rate and under high hydrostatic pressure was reported by Grote *et al*. (2001). Quasi-static compression, SHPB and plate impact experiments were used involving strain rates from 10^{-3} s^{-1} to 10^{4} s^{-1} and confining pressure from 0 to 1·5 GPa. The following formulae were suggested to measure the strain rate dependent DIF.

$$\text{DIF} = 0{\cdot}0235\log_{10}\dot{\varepsilon} + 1{\cdot}07 \quad \text{for } \dot{\varepsilon} \leq 266\ \text{s}^{-1} \quad (7)$$

$$\text{DIF} = 0{\cdot}882(\log_{10}\dot{\varepsilon})^3 - 4{\cdot}4(\log_{10}\dot{\varepsilon})^2 + 7{\cdot}22(\log_{10}\dot{\varepsilon}) - 2{\cdot}64 \quad \text{for } \dot{\varepsilon} > 266\ \text{s}^{-1} \quad (8)$$

Li and Meng (2003) examined SHPB application to determine the dynamic strength of concrete-like materials whose compressive strength is dependent on hydrostatic stress. They showed that the apparent dynamic strength enhancement beyond a strain rate of 10^2 s^{-1} is strongly influenced by the hydrostatic stress effect due to lateral inertia confinement. The following equations were derived to calculate DIF in compression.

$$\text{DIF} = 1 + (\log_{10}\dot{\varepsilon} + 3) \times 0{\cdot}03438 \quad \text{for } \dot{\varepsilon} \leq 100\ \text{s}^{-1} \quad (9)$$

$$\text{DIF} = 8{\cdot}5303 - 7{\cdot}1372\ \log_{10}\dot{\varepsilon} + 1{\cdot}729\ (\log_{10}\dot{\varepsilon})^2 \quad \text{for } \dot{\varepsilon} > 100\ \text{s}^{-1} \quad (10)$$

Zhou and Hao (2008) developed a homogenous and meso-scale model to analyse the behaviour of concrete-like material under high strain rate compression. Both strain rate insensitive and sensitive materials were considered in the numerical model to quantify the relative contribution of the inertia effect and the strain rate effect on the compressive strength DIF. The compressive DIF was proposed as

$$\text{DIF} = 0{\cdot}0225\log_{10}\dot{\varepsilon} + 1{\cdot}12 \quad \text{for } \dot{\varepsilon} \leq 10\ \text{s}^{-1} \quad (11)$$

$$\text{DIF} = 0{\cdot}2713(\log_{10}\dot{\varepsilon})^2 - 0{\cdot}3563(\log_{10}\dot{\varepsilon}) + 1{\cdot}2275 \quad \text{for } 10 \leq \dot{\varepsilon} \leq 2000\ \text{s}^{-1} \quad (12)$$

The dynamic compressive strength of concrete under high strain rates is given by CEB model code 2010 (CEB, 2010) as

$$f_{\text{c,imt,k}}/f_{\text{cm}} = (\dot{\varepsilon}_{\text{c}}/\dot{\varepsilon}_{\text{c0}})^{0{\cdot}014} \quad \text{for } \dot{\varepsilon}_{\text{c}} \leq 30\ \text{s}^{-1}$$
$$f_{\text{c,imt,k}}/f_{\text{cm}} = 0{\cdot}012(\dot{\varepsilon}_{\text{c}}/\dot{\varepsilon}_{\text{c0}})^{1/3} \quad \text{for } \dot{\varepsilon}_{\text{c}} > 30\ \text{s}^{-1} \quad (13)$$

where f_{cm} is the mean compressive strength of concrete, $\dot{\varepsilon}_{\text{c}}$ is the concrete compressive strain rate, valid in the range of 30×10^{-6} s^{-1} to 300 s^{-1} and $\dot{\varepsilon}_{\text{c0}} = 30 \times 10^{-6}$ s^{-1} is the static compressive strain rate.

Tension

The DIF for tension as per CEB model code 1990 (CEB, 1993) is

$$\text{DIF} = \begin{cases} (\dot{\varepsilon}/\dot{\varepsilon}_{\text{s}})^{1{\cdot}016\,\delta_{\text{s}}} & \text{for } \dot{\varepsilon} \leq 30\ \text{s}^{-1} \\ \beta_{\text{s}}(\dot{\varepsilon}/\dot{\varepsilon}_{\text{s}})^{1/3} & \text{for } \dot{\varepsilon}_{\text{s}} > 30\ \text{s}^{-1} \end{cases} \quad (14)$$

where $\dot{\varepsilon}$ is the strain rate in the range of 3×10^{-6} s^{-1} to 300 s^{-1}, $\dot{\varepsilon}_{\text{s}} = 3 \times 10^{-6}$ s^{-1} is the static strain rate and $\log\beta_{\text{s}} = 7{\cdot}11\delta - 2{\cdot}33$, in which $\delta_{\text{s}} = 1/(10 + 6\ f_{\text{cs}}/f_{\text{co}})$ where

$f_{co} = 10$ MPa and f_{cs} is the static compressive strength of concrete.

However, Malvar and Ross (1998) found that the available data in the literature and their additional new data on concrete in tension differed somewhat from the CEB model code 1990 (CEB, 1993) recommendations, mostly for strain rates beyond 1 s^{-1}. They thus modified the DIF equations with a change in slope occurring at a strain rate of 1 s^{-1} instead of 30 s^{-1}. The proposed formulations are

$$15.\quad \mathrm{DIF} = \begin{cases} (\dot{\varepsilon}/\dot{\varepsilon}_s)^{\delta} & \text{for } \dot{\varepsilon} \leq \text{ s}^{-1} \\ \beta(\dot{\varepsilon}/\dot{\varepsilon}_s)^{1/3} & \text{for } \dot{\varepsilon}_s > 1 \text{ s}^{-1} \end{cases}$$

where $\dot{\varepsilon}$ is the strain rate in the range of 10^{-6} s^{-1} to 160 s^{-1}, $\dot{\varepsilon}_s = 10^{-6}$ s^{-1} is the static strain rate and $\log \beta = 6\delta - 2$, with $\delta = 1/(1 + 8\, f_{cs}/f_{co})$ and f_{co} and f_{cs} as before.

Tedesco *et al.* (1997) conducted a series of dynamic tensile tests and, based on the results, proposed the following equations.

$$16.\quad \mathrm{DIF} = 0{\cdot}1425 \log_{10} \dot{\varepsilon} + 1{\cdot}833 \geq 1{\cdot}0 \quad \text{for } \dot{\varepsilon} \leq 2{\cdot}32 \text{ s}^{-1}$$

$$17.\quad \mathrm{DIF} = 2{\cdot}929 \log_{10} \dot{\varepsilon} + 0{\cdot}814 \leq 6 \quad \text{for } \dot{\varepsilon} > 2{\cdot}32 \text{ s}^{-1}$$

The tensile DIF proposed by Zhou and Hao (2008) is

$$18.\quad \mathrm{DIF} = 0{\cdot}0225 \log_{10} \dot{\varepsilon} + 1{\cdot}12 \quad \text{for } \dot{\varepsilon} \leq 0{\cdot}1 \text{ s}^{-1}$$

$$19.\quad \mathrm{DIF} = 0{\cdot}7325(\log_{10} \dot{\varepsilon})^2 + 1{\cdot}235(\log_{10} \dot{\varepsilon}) + 1{\cdot}6 \quad \text{for } 0{\cdot}1 \leq \dot{\varepsilon} \leq 50 \text{ s}^{-1}$$

Xiao *et al.* (2010) performed dynamic tensile testing of plain concrete specimens with axial strain rate ranging from 10^{-5} s^{-1} to 10^{-1} s^{-1}. Compared with the quasi-static strain rate of 10^{-5} s^{-1}, the dynamic tensile strength of concrete at strain rates of 10^{-4} s^{-1}, 10^{-3} s^{-1}, 10^{-2} s^{-1} and 10^{-1} s^{-1} was found to increase by 6·3%, 13·1%, 20·5% and 25·5% respectively. They concluded that this result was similar to the findings of several other researchers. From the test results, they suggested

$$20.\quad \mathrm{DIF} = 1{\cdot}0 + 0{\cdot}0653\ \log(\dot{\varepsilon}_t/\dot{\varepsilon}_{ts})$$

where $\dot{\varepsilon}_t$ is the dynamic strain rate and $\dot{\varepsilon}_{ts}$ is the quasi-static strain rate (10^{-5} s^{-1}).

The dynamic tensile strength of concrete under high strain rates was proposed as

$$21.\quad \begin{aligned} f_{ct,imt,k}/f_{ctm} &= (\dot{\varepsilon}_{ct}/\dot{\varepsilon}_{ct0})^{0{\cdot}018} && \text{for } \dot{\varepsilon}_{ct} \leq 10 \text{ s}^{-1} \\ f_{ct,imt,k}/f_{ctm} &= 0{\cdot}0062\ (\dot{\varepsilon}_{ct}/\dot{\varepsilon}_{ct0})^{1/3} && \text{for } \dot{\varepsilon}_{ct} > 10 \text{ s}^{-1} \end{aligned}$$

where f_{cm} is the mean compressive strength of concrete, $\dot{\varepsilon}_{ct}$ is the concrete compressive strain rate, valid in the range of 1×10^{-6} s^{-1} to 300 s^{-1} and $\dot{\varepsilon}_{ct0} = 1 \times 10^{-6}$ s^{-1} is the static compressive strain rate.

It is thus quite clear there are plentiful equations to calculate the DIF of concrete in compression and tension. The compression and tension DIFs calculated using various equations proposed by different researchers are plotted in Figure 1 and Figure 2, and variability among the proposed equations is obvious. Numerous factors may affect the constitutive behaviour and DIF of concrete under varying strain rates, such as

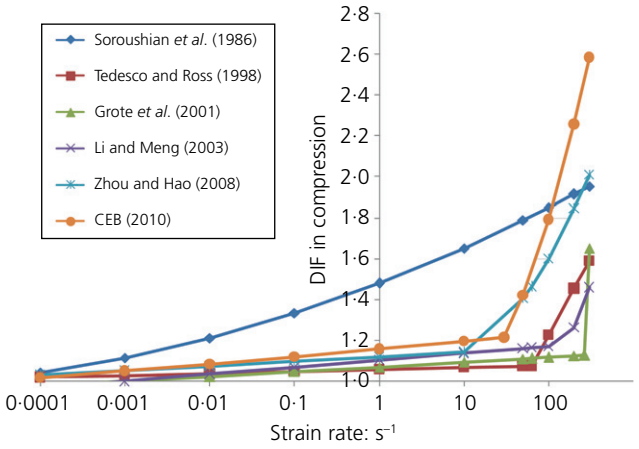

Figure 1. DIF in compression of concrete

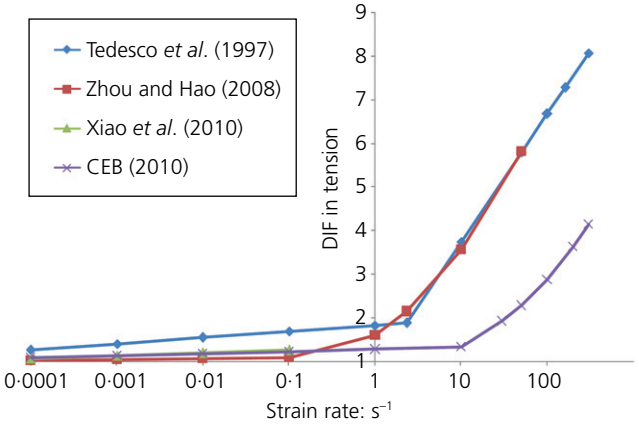

Figure 2. DIF in tension of concrete

mix proportion, cement content, aggregate shape and size, water/cement ratio, age, curing conditions and so on. More test data are thus needed in order to estimate the DIF of concrete strength more precisely and make satisfactory comparisons with existing data in the literature.

Steel reinforcement

Several studies on the effect of strain rate on reinforcing bars, structural steel and steel wires have been documented (Keenan and Feldman, 1960; Soroushian and Choi, 1987; Wakabayashi *et al*., 1980) and detailed reviews of available work have been presented by Fu *et al*. (1991) and Malvar (1998). According to Wakabayashi *et al*. (1980), the yield stress of steel bars increases with increasing strain rate, but the behaviour in the strain-hardening region is not largely affected by strain rate. Soroushian and Choi (1987) concluded that the yield strength of steel is more sensitive to strain rate than the ultimate strength, and that the modulus of elasticity is independent of the rate of straining. According to Soroushian and Choi, the most important factor influencing strain rate effects is the static yield strength, with the mechanical properties of steel of lower yield strength being more sensitive to strain rate than higher yield strength steel. Malvar (1998) reported that the DIF of yield and ultimate stress is inversely related to the yield stress itself. A formulation was proposed to determine the DIF as a function of strain rate and yield stress by fitting available data in the literature. This formulation is valid for yield stresses between 290 MPa and 710 MPa and for strain rates between 10^{-4} s^{-1} and 10 s^{-1} and is given by

$$\text{22.} \quad \text{DIF} = (\dot{\varepsilon}/10^{-4})^{\alpha}$$

where, for yield stress, $\alpha = \alpha_{\text{fy}}$ ($\alpha f_y = 0{\cdot}074 - 0{\cdot}04 f_y/414$) and, for ultimate stress, $\alpha = \alpha_{\text{fu}}$ ($\alpha_{\text{fu}} = 0{\cdot}019 - 0{\cdot}009 f_y/414$), $\dot{\varepsilon}$ is the strain rate in s^{-1} and f_y is the static yield strength of the reinforcement in MPa.

Reinforced concrete beams under impact loading: experimental investigations

Hughes and Beeby (1982) conducted a drop-weight impact test programme comprising 80 pin-ended and 12 simply supported beams. Two impactors of masses 58·5 kg and 98 kg were used, and the impact velocity was varied in the range 2·1–7·9 m/s. Various pads (steel, rubber and plywood) were placed at the impact zone to vary its stiffness. Most of the tested beams failed in flexure at midspan, while two beams (those provided with fewer transverse reinforcements than recommended by the British standard) failed in shear at approximately third points. This was a consequence of the high shear at these points caused by excitation of the third mode. The test results indicated that a high impact velocity (the maximum in the considered range) and a stiff (steel) pad resulted in shear dominant behaviour.

Kishi *et al*. (2001) conducted drop-weight impact tests on eight RC beams to establish a rational impact-resistant design procedure for flexural failure type specimens. Impact load was imparted onto the midspan of specimens by a free-falling 200 kg steel impactor. This work suggested that flexural failure type beams under impact load may be designed with a margin of safety by assuming a dynamic response ratio of 2·0 and a ratio of absorbed energy to input kinetic energy of 0·7. Here, the reaction force versus displacement loop at failure was simplified as a parallelogram, as shown in Figure 3. A simple equation was proposed to calculate the required static bending resistance of beams against impact loading

$$\text{23.} \quad P_{\text{usd}} = 0{\cdot}35 \frac{E_{\text{kd}}}{\delta_{\text{rd}}}$$

in which P_{usd} is the static bending resistance, E_{kd} is the input kinetic energy and δ_{rd} is the residual displacement.

Kishi *et al*. (2002) carried out falling-weight impact tests on shear failure type RC beams to establish a rational impact-resistant design procedure. An impact load was applied at the midspan of the beam by dropping a free-falling 300 kg steel weight. The authors reported that the effects of the striking face of the impactor on the dynamic response and failure mode of the beam were very small under similar impact velocities. It was recommended that shear failure type beams without shear reinforcement under impact loading may be designed with a certain safety margin by assuming a dynamic response ratio of 1·5 and an absorbed input energy ratio of 0·6. The required static shear resistance for beams against impact loading was evaluated by the simple equation

$$\text{24.} \quad V_{\text{usd}} = 0{\cdot}8 \frac{E_{\text{kd}}}{\delta_{\text{rd}}}$$

in which V_{usd} is the static shear resistance, E_{kd} is the input kinetic energy and δ_{rd} is residual displacement.

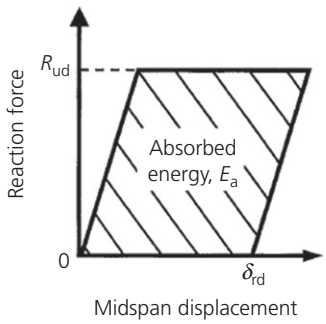

Figure 3. Simplified model for reaction force versus displacement loop (Kishi *et al*. 2001)

Fujikake *et al*. (2009) examined the impact responses of 12 RC beams through an experimental study involving drop-hammer impact tests. A hammer of mass 400 kg was dropped freely onto the top surface of a beam at midspan from four different heights. It was concluded that beams with comparatively lower amounts of longitudinal steel reinforcement exhibited only overall flexural failure, while beams with higher amounts of longitudinal reinforcement not only exhibited overall flexural failure but also showed local failure (i.e. crushing of concrete) near the impact loading point. Local failure was substantially reduced when the beam contained heavy longitudinal compression reinforcement. Impact response characteristics such as the maximum impact load, impulse, duration of impact load, maximum midspan deflection and the time taken for maximum midspan deflection increased as the drop height was increased. However, the duration of the impact load, the maximum midspan deflection and the time taken for the maximum midspan deflection were affected by the flexural rigidity of the beams. Moreover, design guidelines were provided for RC beams under impact loading in the form of a flowchart, as shown in Figure 4.

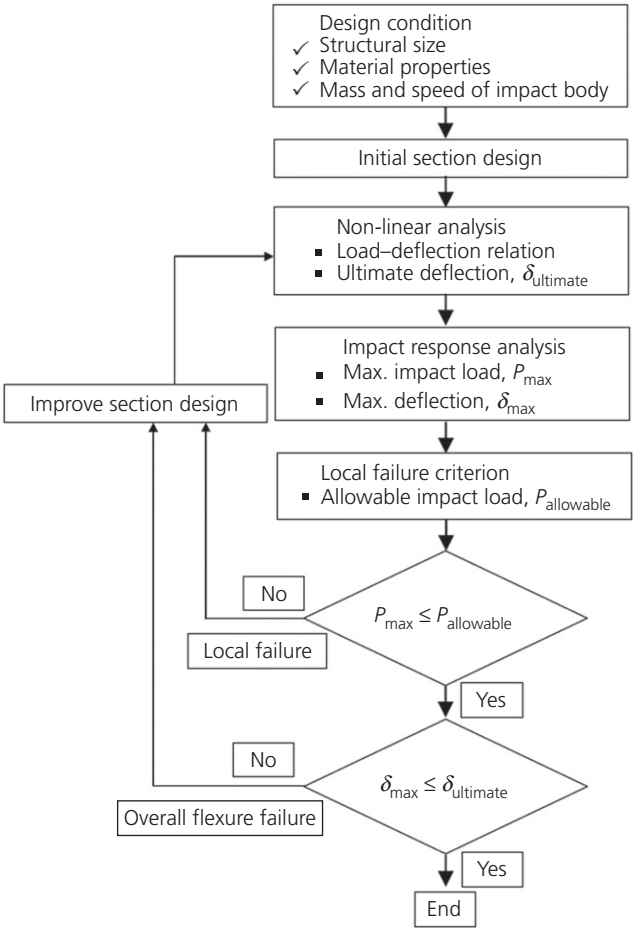

Figure 4. Design flow chart of RC beam subjected to impact loadings (Fujikake *et al*. 2009)

Chen and May (2009) designed a test programme to investigate high-mass and low-velocity impact behaviour of RC beams. All the tests were conducted with a drop-weight of 98·7 kg with an impact velocity of 7·3 m/s. The test variables in this investigation were the support conditions (e.g. pin-ended or simply supported), type of impactor (e.g. hemispherical or flat) and the impact interface (e.g. plywood placed between the beam and impactor or direct impact). The test results revealed that the support conditions had less influence on the impact force than the span length. Moreover, it was concluded that the plywood interface distributed the impact force in a similar manner to the use of a flat impactor.

Saatci and Vecchio (2009) reported on a well-instrumented experimental programme that aimed to contribute towards understanding of the effects of shear mechanisms on the behaviour of RC beams under impact loading. Two different drop-weights (211 kg and 600 kg) were used for impact testing. Regardless of the projected static behaviour of beams, all the specimens developed severe diagonal cracks, originating at the impact point and propagating downwards with an angle of approximately 45°, forming shear plugs. It was thus suggested that shear mechanisms must be considered during the development of methods to predict impact responses. Impact forces at the initial stages of response were mainly resisted by the inertia of the specimens before the forces reached the supports. Therefore, the mass and geometric properties of a structure, such as the beam span length, are important factors in resisting impact forces. Finally, based on experience from the test programme, some recommendations for future experimental studies on impact loading were provided.

Tachibana *et al*. (2010) documented a series of low-speed impact experiments on RC beams with varying span lengths, cross-sections and longitudinal reinforcements. Steel weights of various masses (150, 300 and 450 kg) were employed in the test programme. The following equation was proposed to calculate the maximum midspan deflection of the beam based on impact energy and static ultimate flexure resistance

$$\delta_{max} = 0{\cdot}522\frac{E_{col}}{P_u} \quad (25)$$

where δ_{max} is maximum displacement (mm), E_{col} is kinetic energy (J) and P_u is ultimate flexural resistance (kN). The validity of the proposed equation was corroborated through comparisons with other experimental results and numerical results from finite-element simulations. The static bending resistance of the considered beams ranged from 16·7 kN to 66·7 kN and the impact energies varied from 150 J to 5400 J based on variations of mass and impact velocity.

Kishi and Mikami (2012) developed an impact-resistance design methodology for RC beams following performance-based design based on falling-weight impact test results. Three different drop-hammer masses were used (300, 400 and 500 kg) and impact velocities were in the range 3·1–7·7 m/s. Flexural cracks were observed not only in the bottom fibre but also in the upper fibre throughout the clear span. Moreover, diagonal shear cracks formed around the midspan area, mainly below the impact point, and these cracks became prominent with increasing impact velocity. On the basis of the relationships between maximum and residual deflections per unit input impact energy E, the following empirical design formulae were proposed

$$26. \quad P_{usc} = 0{\cdot}63\frac{E}{D_{max}}$$

$$27. \quad P_{usc} = 0{\cdot}42\frac{E}{\delta_{rs}}$$

in which P_{usc} is the static flexural load carrying capacity (kN), E is input impact energy (J), D_{max} is the maximum displacement and δ_{rs} is the residual displacement (mm). These two equations allow for a significant simplification in design approach for structures subjected to impact loading. However, there are some limitations in the application – an input impact energy $E < 15$ kJ and applicability to RC beams having a static flexural load carrying capacity $P_{usc} < 240$ kN and static shear flexural capacity ratio $\alpha > 1{\cdot}5$.

An impact test programme on 30 RC beams was conducted by the current authors (Adhikary *et al*., 2015) to examine impact response and failure modes. The test results showed that no shear failure occurred under impact loading in statically flexure-critical beams (i.e. shear to bending resistance ratio greater than one). However, with increasing drop height, more localised failure with extensive concrete crushing at the impact region was observed. On the contrary, a transition in the mode of failure of RC beams from flexural failure at static loading to shear failure at low-velocity impact has been reported in the literature (Hughes and Beeby, 1982; Saatci and Vecchio, 2009). The impact interface (i.e. direct impact or with some interface such as a steel or plywood plate between the impactor and the beam) could be one reason why this change in failure mode was not observed in the test programme conducted by Adhikary *et al*. (2015). A harder and stiffer contact zone (e.g. when a steel plate is placed between the impactor and the beam) produces more inertia forces (i.e. the majority of impact energy transfers to the beam through the steel plate, which accelerates the beam in the direction of the impact force generating more inertia force), which helps the beam to fail in shear under impact loading. However, in the test programme of Adhikary *et al*. (2015), due to the direct contact of the impactor with the beam during the impact event, the majority of the impact energy was dissipated during localised crushing of concrete in the impact region, thus developing less inertia force due to less energy transfer to the entire span of the beam.

Analysis of experimental database

A database of RC beams tested under drop-weight impact loading was compiled from the literature (Bhatti *et al*., 2009; Chen and May, 2009; Fujikake *et al*., 2009; Kishi *et al*., 2001, 2002); Kishi and Mikami, 2012; Saatci and Vecchio, 2009; Tachibana *et al*., 2010) and is concisely tabulated in Appendix 1 and 2.

Tachibana *et al*. (2010) proposed an equation to estimate the maximum midspan deflection of beams based on impact energy and static flexural resistance. Similarly, empirical design formulae following the performance-based design concept were suggested by Kishi and Mikami (2012), which involved the static flexural resistance, maximum and /or residual deflection and input impact energy. As limited databases were employed in the above-mentioned research studies, efforts were devoted here to finding relationships among static resistance (both flexure and shear), maximum midspan deflection and input impact energy by using data documented by several research studies reported in the literature.

The compiled database comprises 174 beams tested under drop-weight impact loading at their midspan (details of some of the beams are not available in the literature). The beam details, material properties and static shear to bending resistance ratio are tabulated in Appendix 1. Out of the 174 specimens, 53 were of static shear failure type and the remaining 121 were static flexural failure type beams. All impact responses were sorted based on their first impact. The mass of the impactor, impact velocity and impact responses are succinctly presented in Appendix 2. The geometry of the test specimens, amounts of longitudinal and shear reinforcement, the compressive strength of the concrete and the yield strength of the longitudinal reinforcement span a wide range. All the beams were of rectangular cross-section, with dimensions in the range 100–300 mm width, 150–560 mm height and 1–4 m clear span length. The longitudinal reinforcement ratio varied from 0·84% to 2·75%, whereas the shear reinforcement ratio was in the range 0·11–0·75%. The concrete strength of the specimens was mostly within the range 24–50 MPa. The diameter of longitudinal reinforcements in the test specimens varied from 13–35 mm and the diameter of transverse reinforcements for 90% of the beams was 6 mm. The yield strength of longitudinal reinforcement varied from 345 MPa to 520 MPa. Moreover, various types and shapes of impactors and beam–impactor interfaces were used by different researchers, as shown in Table 1.

Figure 5 shows the relationship between maximum midspan deflection (δ_{max}) versus input impact energy over static flexural

Investigators	Type of impactor	Impact interface
Kishi *et al*. (2001)	Not provided	Not provided
Kishi *et al*. (2002)	Spherical with radius of curvature of 1407 mm	Direct contact
Bhatti *et al*. (2009)	Spherical steel weight with radius of curvature of 1407 mm	Direct contact
Fujikake *et al*. (2009)	Drop hammer with hemispherical tip of radius 90 mm	Direct contact
Chen and May (2009)	Stainless steel with a 90 mm diameter and hemispherical profile of 125 mm radius Mild steel with a 100 mm diameter and flat contact surface	12 mm plywood and direct contact
Saatci and Vecchio (2009)	305 mm square hollow structural steel weight	50 mm thick 305 mm square steel plate
Tachibana *et al*. (2010)	Steel weight with a curved contact surface, length 565 mm, radius 75 mm	Direct contact
Kishi and Mikami (2012)	Steel weight with a spherical bottom of radius 1407 mm and 2 mm taper	Direct contact

Table 1. Type of impactor and beam–impactor interface used in the experimental works

resistance (E/R_b). About 90 out of the 121 experimental specimens of static flexural failure type are plotted in Figure 5 as there was insufficient experimental data given for the remaining 31 specimens. The static bending resistance of the considered beams varied from 11·4 kN to 237·5 kN and the input impact energy varied from 0·1 kJ to 19·2 kJ due to the variations in impactor mass (98·7–600 kg) and impact velocity (1–8 m/s). Although there were variations in beam geometry, type of impactor and beam–impactor interface, the values of maximum midspan deflection fit well with the linear line. However, the proposed equation (FC9) can only be applied up to $E/R_b = 150$. More data is thus required in order to extend the applicability of the equation beyond this value of E/R_b. Similarly, for statically shear-critical beams, the relationship between maximum midspan deflection (δ_{max}) and input impact energy over static shear resistance (E/R_s) is shown in Figure 6. As mentioned earlier, there was insufficient impact response data for some shear failure type beams from the database, thus the data points shown in Figure 6 only cover 42 out of the 53 specimens. The input impact energy varied from 0·15 kJ to 19·2 kJ due to variations in mass of the impactor (98·7–600 kg) and impact velocity (1–9·3 m/s). It was observed

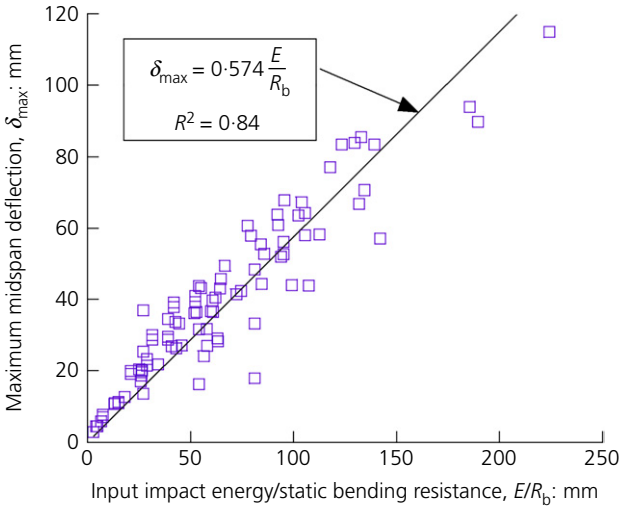

Figure 5. Relationship between maximum midspan deflection and input impact energy over static flexural resistance

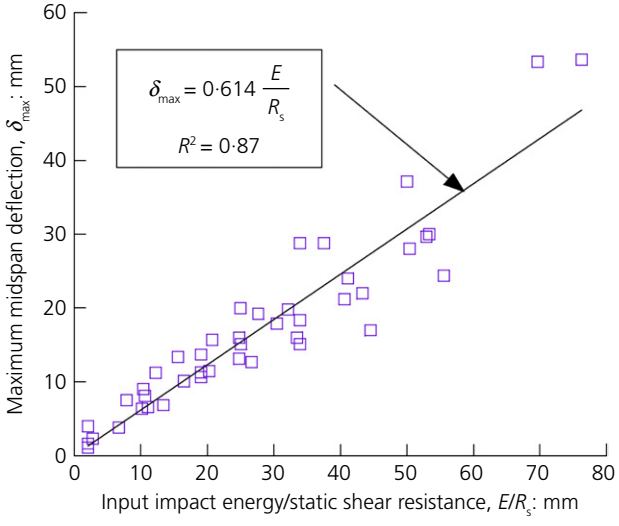

Figure 6. Relationship between maximum midspan deflection and input impact energy over static shear resistance

that the maximum displacement can be accurately predicted using the equation proposed in the figure, but more data are essential in order to extend the applicability of the equation beyond $E/R_s = 50$.

Empirical formulae for impact-resistant design

Two empirical equations can be proposed from the aforementioned analysis of the experimental database.

For static flexural failure type beams

$$R_b = 0{\cdot}574\frac{E}{\delta_{max}} \quad (28)$$

and for static shear failure type beams

$$R_s = 0{\cdot}614\frac{E}{\delta_{max}} \quad (29)$$

where R_b and R_s are in kN, E is in J and δ_{max} is in mm.

Therefore, by specifying the maximum midspan deflection (δ_{max}) for each limit state of the beam, the required static bending (R_b) or shear resistance (R_s) for impact-resistant design can be determined by applying Equations 28 and 29. To demonstrate the applicability of the proposed equations, comparisons were made with the test results provided by Adhikary *et al.* (2015). Figure 7 (for flexure-critical beams) and Figure 8 (for shear-critical beams) show the comparative plots of the experimental results of maximum deflection with the proposed equations. The figures show good agreement, and the two proposed equations could thus be used in design with the aforementioned limitations.

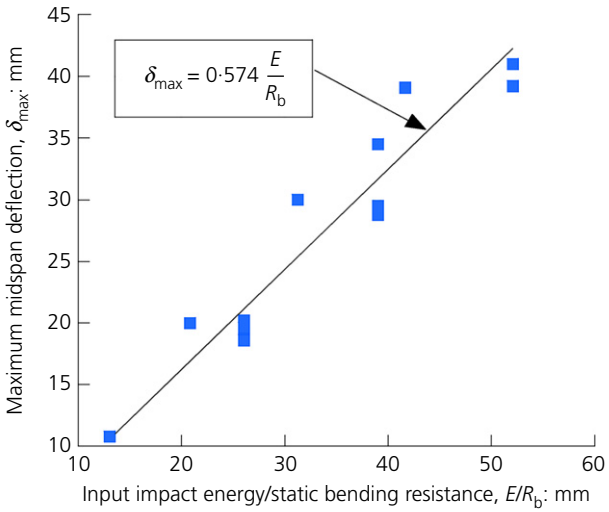

Figure 7. Comparison of test results (Adhikary *et al.*, 2015) with proposed equation for flexure-critical beams

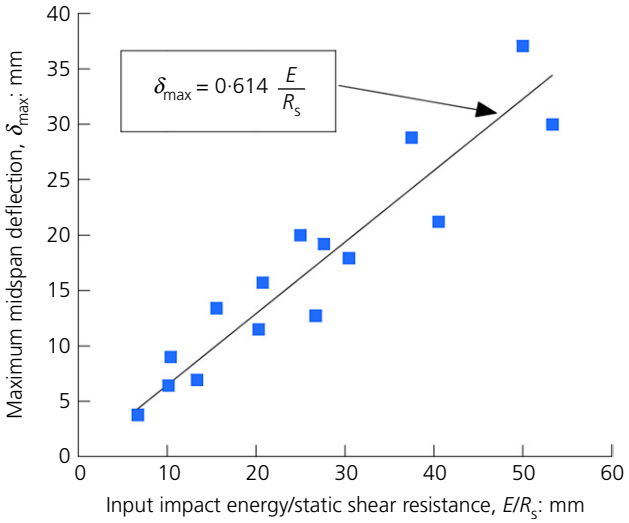

Figure 8. Comparison of test results (Adhikary *et al.*, 2015) with proposed equation for shear-critical beams

The equations proposed for static flexural failure type beams by Tachibana *et al.* (2010) and Kishi and Mikami (2012) are similar to the proposed equation (Equation 28) apart from the constant values, which were specified as 0·522 and 0·63 by Tachibana *et al.* (2010) and Kishi and Mikami (2012) respectively. The constant in Equation 28 is 0·574, which is very close to the average of the two previously proposed values; therefore Equation 28 gives a less conservative but more economical calculation of required static bending resistance compared with Kishi and Mikami (2012) and vice versa for Tachibana *et al.* (2010). Although there are some variations in beam dimensions, test setup, type of impactor and impactor interface in the research works studied, it can be concluded that the required static bending resistance for impact-resistant design is highly dependent on input impact energy and the limit state of maximum midspan deflection.

The required static shear resistance for a static shear failure type beam against impact loading can be evaluated by the simple equation proposed by Kishi *et al.* (2002)

$$V_{usd} = 0{\cdot}8\frac{E_{kd}}{\delta_{rd}} \quad (30)$$

where V_{usd} is static shear resistance, E_{kd} is input kinetic energy and δ_{rd} is residual displacement. The constant value in Equation 30 is 0·8 whereas the proposed equation (Equation 29) suggests a constant value of 0·614. The discrepancy is due to the fact that Kishi *et al.* (2002) considered the limit state of residual deflection (δ_{rd}) as an input parameter while Equation 29 considers the limit state of maximum midspan deflection (δ_{max}). It is therefore difficult to directly compare these two equations.

Conclusions and future research directions

(*a*) A comprehensive review of the strain rate effects on concrete mechanical properties has been presented and it has been shown that there are numerous equations in the literature to calculate the dynamic increase factor (DIF) of concrete in compression and tension. Numerous factors may affect the constitutive behaviour and DIF of concrete under varying strain rates, such as mix proportion, cement content, aggregate shape and size, water/cement ratio, age, curing conditions and so on. More test data are thus needed to estimate the DIF of concrete strength more precisely and make a comparison with existing data in the literature. Moreover, there seems to be a lack of general consensus on whether the strain rate enhancement of concrete strength is a material effect or a structural effect. Further research is needed to examine this issue.

(*b*) Two empirical equations are proposed from analysis of an extensive dataset of RC beams under drop-weight impact loading documented by several researchers in the literature. By specifying the maximum midspan deflection for each limit state of a beam, the required static bending and shear resistance can be determined for designing a beam subjected to input impact energy. To demonstrate the applicability of the proposed equations, a comparison was made with results from tests conducted by the authors.

(*c*) An increased tendency towards shear failure of RC beams under impact loading has been mentioned by several researchers (Hughes and Beeby, 1982; Saatci and Vecchio, 2009) although, under static loading, the beams failed in flexure. The reason for this is the presence of inertia forces, which are responsible for different deflected shapes and subsequently a higher shear to moment ratio (i.e. in higher vibration modes). The impact interface plays an important role in developing the severity of inertia forces. A harder and stiffer contact zone (e.g. when a steel plate is placed between the impactor and the beam) produces more inertia forces (i.e. the majority of impact energy transfers to the beam through the steel plate, which accelerates the beam in the direction of the impact force, generating more inertia force), which will assist the beam to fail in shear under impact loading. In the test programme conducted by the authors (Adhikary *et al.*, 2015), no shear failure occurred in statically flexure-critical beams, but more localised failure with extensive concrete crushing below the impactor was observed with increasing drop-height. Due to the direct contact of the impactor with the beam during the impact event, the majority of impact energy was dissipated during localised crushing of the concrete in the impact region, thus developing less inertia force due to reduced energy transfer to the entire span of the beam. Future research should focus on the issue of whether the failure mode of statically flexure-critical beams under impact loading (i.e. direct contact) changes to shear or not (or localised failure governs).

(*d*) For a more thorough comparative study, research initiatives should also be undertaken to test identical specimens (i.e. similar not only at the structural level but also at the material level (e.g. aggregate size, compressive strength of concrete and yield strength of reinforcements)) using different drop-weight impact machines (i.e. also keeping the impactor shape and size, impact interface and boundary conditions almost identical). Moreover, the data acquisition systems used should be almost identical in order to facilitate better analysis and comparison of the test results. In general, more efforts are needed to determine the impact resistance of RC beams, considering various structural masses and geometries and various impactor masses and velocities.

Appendix 1 Beam geometry and reinforcement details for drop-weight impact loading

Beam ID	Beam characteristics						a/d	L/h	Longitudinal reinforcement						Shear reinforcement			R_s/R_b
	f'_c: MPa	h: mm	b: mm	d: mm	a: mm	L: mm			Top			Bottom			Diameter: mm	Ratio: %	f_{Ty}: MPa	
									Diameter: mm	Ratio: %	f_{Ly}: MPa	Diameter: mm	Ratio: %	f_{Ly}: MPa				
Kishi *et al*. (2001)																		
A19	26·5	240	160	190	1000	2500	5·26	10·42	19	1·88	373	19	1·88	373	6	0·396	373	3·1
A22	26·5	240	160	190	1000	2500	5·26	10·42	22	2·55	373	22	2·55	373	6	0·396	373	1·9
B10	26·5	220	200	170	1000	2500	5·88	11·36	10	0·42	373	10	0·42	373	6	0·317	373	5·85
B13	26·5	220	200	170	1000	2500	5·88	11·36	13	0·75	373	13	0·75	373	6	0·317	373	3·96
B19	26·5	220	200	170	1000	2500	5·88	11·36	19	1·69	373	19	1·69	373	6	0·317	373	2·13
C10	26·5	160	160	120	1000	2500	8·33	15·63	10	0·74	373	10	0·74	373	6	0·396	373	6·04
C13	26·5	160	160	120	1000	2500	8·33	15·63	13	1·32	373	13	1·32	373	6	0·396	373	4·36
C19	26·5	160	160	120	1000	2500	8·33	15·63	19	2·98	373	19	2·98	373	6	0·396	373	2·3
Kishi *et al*. (2002)																		
A24	33	250	150	210	500	1400	2·4	5·6	n/a	n/a	n/a	19	1·8	393	n/a	n/a	n/a	0·43
	33	250	150	210	500	1400	2·4	5·6	n/a	n/a	n/a	19	1·8	393	n/a	n/a	n/a	0·43
	33	250	150	210	500	1400	2·4	5·6	n/a	n/a	n/a	19	1·8	393	n/a	n/a	n/a	0·43
	33	250	150	210	500	1400	2·4	5·6	n/a	n/a	n/a	19	1·8	393	n/a	n/a	n/a	0·43
	33	250	150	210	500	1400	2·4	5·6	n/a	n/a	n/a	19	1·8	393	n/a	n/a	n/a	0·43
A36	33	250	150	210	750	1900	3·6	7·6	n/a	n/a	n/a	19	1·8	393	n/a	n/a	n/a	0·64
	33	250	150	210	750	1900	3·6	7·6	n/a	n/a	n/a	19	1·8	393	n/a	n/a	n/a	0·64
	33	250	150	210	750	1900	3·6	7·6	n/a	n/a	n/a	19	1·8	393	n/a	n/a	n/a	0·64
	33	250	150	210	750	1900	3·6	7·6	n/a	n/a	n/a	19	1·8	393	n/a	n/a	n/a	0·64
A48	33	250	150	210	1000	2400	4·8	9·6	n/a	n/a	n/a	19	1·8	393	n/a	n/a	n/a	0·86
	33	250	150	210	1000	2400	4·8	9·6	n/a	n/a	n/a	19	1·8	393	n/a	n/a	n/a	0·86
	33	250	150	210	1000	2400	4·8	9·6	n/a	n/a	n/a	19	1·8	393	n/a	n/a	n/a	0·86
	33	250	150	210	1000	2400	4·8	9·6	n/a	n/a	n/a	19	1·8	393	n/a	n/a	n/a	0·86
B24	33	250	150	210	500	1400	2·4	5·6	n/a	n/a	n/a	13	0·84	393	n/a	n/a	n/a	0·68
	33	250	150	210	500	1400	2·4	5·6	n/a	n/a	n/a	13	0·84	393	n/a	n/a	n/a	0·68
	33	250	150	210	500	1400	2·4	5·6	n/a	n/a	n/a	13	0·84	393	n/a	n/a	n/a	0·68
	33	250	150	210	500	1400	2·4	5·6	n/a	n/a	n/a	13	0·84	393	n/a	n/a	n/a	0·68
	33	250	150	210	500	1400	2·4	5·6	n/a	n/a	n/a	13	0·84	393	n/a	n/a	n/a	0·68
B36	33	250	150	210	750	1900	3·6	7·6	n/a	n/a	n/a	13	0·84	393	n/a	n/a	n/a	1·03
	33	250	150	210	750	1900	3·6	7·6	n/a	n/a	n/a	13	0·84	393	n/a	n/a	n/a	1·03
	33	250	150	210	750	1900	3·6	7·6	n/a	n/a	n/a	13	0·84	393	n/a	n/a	n/a	1·03
	33	250	150	210	750	1900	3·6	7·6	n/a	n/a	n/a	13	0·84	393	n/a	n/a	n/a	1·03

(continued on next page)

Beam ID	Beam characteristics						a/d	L/h	Longitudinal reinforcement						Shear reinforcement			R_s/R_b
	f'_c: MPa	h: mm	b: mm	d: mm	a: mm	L: mm			Top			Bottom			Diameter: mm	Ratio: %	f_{Ty}: MPa	
									Diameter: mm	Ratio: %	f_{Ly}: MPa	Diameter: mm	Ratio: %	f_{Ly}: MPa				
B48	33	250	150	210	1000	2400	4·8	9·6	n/a	n/a	n/a	13	0·84	393	n/a	n/a	n/a	1·37
	33	250	150	210	1000	2400	4·8	9·6	n/a	n/a	n/a	13	0·84	393	n/a	n/a	n/a	1·37
	33	250	150	210	1000	2400	4·8	9·6	n/a	n/a	n/a	13	0·84	393	n/a	n/a	n/a	1·37
	33	250	150	210	1000	2400	4·8	9·6	n/a	n/a	n/a	13	0·84	393	n/a	n/a	n/a	1·37
	33	250	150	210	1000	2400	4·8	9·6	n/a	n/a	n/a	13	0·84	393	n/a	n/a	n/a	1·37
Bhatti *et al.* (2009)																		
A37	41·2	400	200	350	1000	2400	2·86	6	35	2·75	373	35	2·75	373	6	0·21	373	0·57
A46	41·2	400	200	350	1000	2400	2·86	6	35	2·75	373	35	2·75	373	6	0·21	373	0·57
A56	41·2	400	200	350	1000	2400	2·86	6	35	2·75	373	35	2·75	373	6	0·21	373	0·57
A65	41·2	400	200	350	1000	2400	2·86	6	35	2·75	373	35	2·75	373	6	0·21	373	0·57
A74	41·2	400	200	350	1000	2400	2·86	6	35	2·75	373	35	2·75	373	6	0·21	373	0·57
A84	41·2	400	200	350	1000	2400	2·86	6	35	2·75	373	35	2·75	373	6	0·21	373	0·57
B37	41·2	400	200	350	1000	2400	2·86	6	35	2·75	373	35	2·75	373	6	0·42	373	0·76
B46	41·2	400	200	350	1000	2400	2·86	6	35	2·75	373	35	2·75	373	6	0·42	373	0·76
B65	41·2	400	200	350	1000	2400	2·86	6	35	2·75	373	35	2·75	373	6	0·42	373	0·76
B74	41·2	400	200	350	1000	2400	2·86	6	35	2·75	373	35	2·75	373	6	0·42	373	0·76
B84	41·2	400	200	350	1000	2400	2·86	6	35	2·75	373	35	2·75	373	6	0·42	373	0·76
B93	41·2	400	200	350	1000	2400	2·86	6	35	2·75	373	35	2·75	373	6	0·42	373	0·76
Fujikake *et al.* (2009)																		
S1616	42	250	150	210	700	1700	3·3	6·8	16	1·28	426	16	1·28	426	10	1·4	295	2·55
	42	250	150	210	700	1700	3·3	6·8	16	1·28	426	16	1·28	426	10	1·4	295	2·55
	42	250	150	210	700	1700	3·3	6·8	16	1·28	426	16	1·28	426	10	1·4	295	2·55
	42	250	150	210	700	1700	3·3	6·8	16	1·28	426	16	1·28	426	10	1·4	295	2·55
S1322	42	250	150	210	700	1700	3·3	6·8	13	0·84	397	22	2·41	418	10	1·4	295	1·51
	42	250	150	210	700	1700	3·3	6·8	13	0·84	397	22	2·41	418	10	1·4	295	1·51
	42	250	150	210	700	1700	3·3	6·8	13	0·84	397	22	2·41	418	10	1·4	295	1·51
	42	250	150	210	700	1700	3·3	6·8	13	0·84	397	22	2·41	418	10	1·4	295	1·51

(continued on next page)

Beam ID	Beam characteristics						a/d	L/h	Longitudinal reinforcement						Shear reinforcement			R_s/R_b
									Top			Bottom						
	f'_c: MPa	h: mm	b: mm	d: mm	a: mm	L: mm			Diameter: mm	Ratio: %	f_{Ly}: MPa	Diameter: mm	Ratio: %	f_{Ly}: MPa	Diameter: mm	Ratio: %	f_{Ty}: MPa	
S2222	42	250	150	210	700	1700	3·3	6·8	22	2·41	418	22	2·41	418	10	1·4	295	1·51
	42	250	150	210	700	1700	3·3	6·8	22	2·41	418	22	2·41	418	10	1·4	295	1·51
	42	250	150	210	700	1700	3·3	6·8	22	2·41	418	22	2·41	418	10	1·4	295	1·51
	42	250	150	210	700	1700	3·3	6·8	22	2·41	418	22	2·41	418	10	1·4	295	1·51
Chen and May (2009)																		
A1	49·2	200	100	175	1350	3000	7·7	15	6	0·32	510	12	1·29	510	6	0·28	250	1·48
	49·2	200	100	175	1350	3000	7·7	15	6	0·32	510	12	1·29	510	6	0·28	250	1·48
	49·2	200	100	175	1350	3000	7·7	15	6	0·32	510	12	1·29	510	6	0·28	250	1·48
	49·2	200	100	175	1350	3000	7·7	15	6	0·32	510	12	1·29	510	6	0·28	250	1·48
	45·8	200	100	175	1350	3000	7·7	15	6	0·32	510	12	1·29	510	6	0·28	250	1·44
	45·8	200	100	175	1350	3000	7·7	15	6	0·32	510	12	1·29	510	6	0·28	250	1·44
A1	33·6	200	100	175	1350	3000	7·7	15	6	0·32	510	12	1·29	510	6	0·28	250	1·26
A2	45·8	200	100	175	1350	3000	7·7	15	6	0·32	510	12	1·29	510	6	0·28	250	1·44
	42·8	200	100	175	1350	3000	7·7	15	6	0·32	510	12	1·29	510	6	0·28	250	1·38
A3	35·6	200	100	175	750	1800	4·3	9	6	0·32	510	12	1·29	510	6	0·28	250	0·72
B1	33·6	200	100	175	1350	3000	7·7	15	6	0·32	510	12	1·29	510	6	0·28	250	1·26
	33·6	200	100	175	1350	3000	7·7	15	6	0·32	510	12	1·29	510	6	0·28	250	1·26
B1	45·8	200	100	175	1350	3000	7·7	15	6	0·32	510	12	1·29	510	6	0·28	250	1·44
B2	35·6	200	100	175	750	1800	4·3	9	6	0·32	510	12	1·29	510	6	0·28	250	0·72
	35·6	200	100	175	750	1800	4·3	9	6	0·32	510	12	1·29	510	6	0·28	250	0·72
B3	42·8	200	100	175	1350	3000	7·7	15	6	0·32	510	12	1·29	510	6	0·28	250	1·38
B3	33·6	200	100	175	1350	3000	7·7	15	6	0·32	510	12	1·29	510	6	0·28	250	1·26
B4	35·6	200	100	175	750	1800	4·3	9	6	0·32	510	12	1·29	510	6	0·28	250	0·72
Saatci and Vecchio (2009)																		
SS0a	50·1	410	250	357	1500	4880	4·2	11·9	30	1·58	464	30	1·58	464	6	n/a	n/a	0·67
SS0b	50·1	410	250	357	1500	4880	4·2	11·9	30	1·58	464	30	1·58	464	6	n/a	n/a	0·67
SS1a	44·7	410	250	357	1500	4880	4·2	11·9	30	1·58	464	30	1·58	464	6	0·1	605	1·08
SS1b	44·7	410	250	357	1500	4880	4·2	11·9	30	1·58	464	30	1·58	464	6	0·1	605	1·08
SS2a	47	410	250	357	1500	4880	4·2	11·9	30	1·58	464	30	1·58	464	6	0·2	605	1·28
SS2b	47	410	250	357	1500	4880	4·2	11·9	30	1·58	464	30	1·58	464	6	0·2	605	1·28
SS3a	46·7	410	250	357	1500	4880	4·2	11·9	30	1·58	464	30	1·58	464	6	0·3	605	1·89
SS3b	46·7	410	250	357	1500	4880	4·2	11·9	30	1·58	464	30	1·58	464	6	0·3	605	1·89

(continued on next page)

Beam ID	Beam characteristics						a/d	L/h	Longitudinal reinforcement						Shear reinforcement			R_s/R_b
									Top			Bottom						
	f'_c: MPa	h: mm	b: mm	d: mm	a: mm	L: mm			Diameter: mm	Ratio: %	f_{Ly}: MPa	Diameter: mm	Ratio: %	f_{Ly}: MPa	Diameter: mm	Ratio: %	f_{Ty}: MPa	
Tachibana *et al*. (2010)																		
A1	24	250	150	210	500	1400	2·38	5·6	13	0·843	345	13	0·843	345	6	0·75	295	1·4
A2-1	24	250	150	210	1000	2400	4·76	9·6	13	0·843	345	13	0·843	345	6	0·75	295	2·7
A2-2	24	250	150	210	1000	2400	4·76	9·6	13	0·843	345	13	0·843	345	6	0·75	295	2·7
A2-3	24	250	150	210	1000	2400	4·76	9·6	13	0·843	345	13	0·843	345	6	0·75	295	2·7
A2-4	24	250	150	210	1000	2400	4·76	9·6	13	0·843	345	13	0·843	345	6	0·75	295	2·7
A2-5	24	250	150	210	1000	2400	4·76	9·6	13	0·843	345	13	0·843	345	6	0·75	295	2·7
A2-6	24	250	150	210	1000	2400	4·76	9·6	13	0·843	345	13	0·843	345	6	0·75	295	2·7
A2-7	24	250	150	210	1000	2400	4·76	9·6	13	0·843	345	13	0·843	345	6	0·75	295	2·7
A2-8	24	250	150	210	1000	2400	4·76	9·6	13	0·843	345	13	0·843	345	6	0·75	295	2·7
A2-9	24	250	150	210	1000	2400	4·76	9·6	13	0·843	345	13	0·843	345	6	0·75	295	2·7
A2-10	24	250	150	210	1000	2400	4·76	9·6	13	0·843	345	13	0·843	345	6	0·75	295	2·7
A2-11	24	250	150	210	1000	2400	4·76	9·6	13	0·843	345	13	0·843	345	6	0·75	295	2·7
A2-12	24	250	150	210	1000	2400	4·76	9·6	13	0·843	345	13	0·843	345	6	0·75	295	2·7
A2-13	24	250	150	210	1000	2400	4·76	9·6	13	0·843	345	13	0·843	345	6	0·75	295	2·7
A2-14	24	250	150	210	1000	2400	4·76	9·6	13	0·843	345	13	0·843	345	6	0·75	295	2·7
A4	24	250	150	210	2000	4400	3·52	17·6	13	0·843	345	13	0·843	345	6	0·75	295	5·5
B	24	150	300	110	1000	2400	9·09	16	13	0·804	345	13	0·804	345	6	0·37	295	2·1
C	24	250	150	210	1000	2400	4·76	9·6	16	1·277	345	16	1·277	345	6	0·75	295	1·9
D	24	250	150	210	1000	2400	4·76	9·6	10	0·499	345	10	0·499	345	6	0·75	295	4·3
E	24	400	150	360	1000	2400	2·78	6	13	0·492	345	13	0·492	345	6	0·75	295	2·4
F	24	400	150	360	1000	2400	2·78	6	10	0·291	345	10	0·291	345	6	0·75	295	4
Kishi and Mikami (2012)																		
G1-1	33·7	300	200	260	1500	3400	5·77	11·33	19	1·1	379	19	1·1	379	6	0·07	295	2·81
G1-1S	33·7	300	200	260	1500	3400	5·77	11·33	19	1·1	379	19	1·1	379	6	0·07	295	2·81
G2-1	32·2	250	150	210	1000	2400	4·76	9·6	13	0·8	373	13	0·8	373	6	0·13	295	3·67
G2-2	32·2	250	150	210	1000	2400	4·76	9·6	13	0·8	373	13	0·8	373	6	0·13	295	3·67
G2-3	32·2	250	150	210	1000	2400	4·76	9·6	13	0·8	373	13	0·8	373	6	0·13	295	3·67
G2L-1	32·2	250	150	210	1000	2400	4·76	9·6	13	0·8	373	13	0·8	373	6	0·13	295	3·67
G2L-2	32·2	250	150	210	1000	2400	4·76	9·6	13	0·8	373	13	0·8	373	6	0·13	295	3·67
G2L-3	32·2	250	150	210	1000	2400	4·76	9·6	13	0·8	373	13	0·8	373	6	0·13	295	3·67
G3-1	34·6	250	150	210	1000	2400	4·76	9·6	13	0·8	393	13	0·8	393	6	0·13	295	3·51
G3-2	34·6	250	150	210	1000	2400	4·76	9·6	13	0·8	393	13	0·8	393	6	0·13	295	3·51

(continued on next page)

Beam ID	Beam characteristics						a/d	L/h	Longitudinal reinforcement						Shear reinforcement			R_s/R_b
									Top			Bottom						
	f'_c: MPa	h: mm	b: mm	d: mm	a: mm	L: mm			Diameter: mm	Ratio: %	f_{Ly}: MPa	Diameter: mm	Ratio: %	f_{Ly}: MPa	Diameter: mm	Ratio: %	f_{Ty}: MPa	
G3-3	34·6	250	150	210	1000	2400	4·76	9·6	13	0·8	393	13	0·8	393	6	0·13	295	3·51
G4-1	32·3	250	150	210	1000	2400	4·76	9·6	13	0·8	373	13	0·8	373	6	0·13	295	3·52
G4-2	32·3	250	150	210	1000	2400	4·76	9·6	13	0·8	373	13	0·8	373	6	0·13	295	3·52
G5-1	39·2	300	200	260	1500	3400	5·77	11·33	19	1·1	379	19	1·1	379	6	0·07	295	2·85
G5-2	39·2	300	200	260	1500	3400	5·77	11·33	19	1·1	379	19	1·1	379	6	0·07	295	2·85
G6-1	34·7	250	250	210	1000	2400	4·76	9·6	19	1·09	392	19	1·09	392	6	0·13	295	2·19
G7-1	34·7	250	250	210	1500	3400	7·14	13·6	19	1·09	392	19	1·09	392	6	0·09	295	2·78
G7-2	34·7	250	250	210	1500	3400	7·14	13·6	19	1·09	392	19	1·09	392	6	0·09	295	2·78
G8-1	34·7	200	200	160	1000	2400	6·25	12	25	3·17	383	25	3·17	383	6	0·16	295	1·55
G9-1	34·7	200	200	160	1500	3400	9·38	17	25	3·17	383	25	3·17	383	6	0·12	295	2
G9-2	34·7	200	200	160	1500	3400	9·38	17	25	3·17	383	25	3·17	383	6	0·12	295	2
G10-1	23·5	250	200	210	1500	3400	7·14	13·6	19	1·36	404	19	1·36	404	6	0·09	295	5·11
G10-2	23·5	250	200	210	1500	3400	7·14	13·6	19	1·36	404	19	1·36	404	6	0·09	295	5·11
G10-3	23·5	250	200	210	1500	3400	7·14	13·6	19	1·36	404	19	1·36	404	6	0·09	295	5·11
G10-4	23·5	250	200	210	1500	3400	7·14	13·6	19	1·36	404	19	1·36	404	6	0·09	295	5·11
G11-1	23·6	300	200	250	1350	3100	5·4	10·33	22	1·55	401	22	1·55	401	6	0·08	295	1·66
G11-2	23·6	300	200	250	1350	3100	5·4	10·33	22	1·55	401	22	1·55	401	6	0·08	295	1·66
G11-3	23·6	300	200	250	1350	3100	5·4	10·33	22	1·55	401	22	1·55	401	6	0·08	295	1·66
G11-4	23·6	300	200	250	1350	3100	5·4	10·33	22	1·55	401	22	1·55	401	6	0·08	295	1·66
G11-5	23·6	300	200	250	1350	3100	5·4	10·33	22	1·55	401	22	1·55	401	6	0·08	295	1·66
G11-6	23·6	300	200	250	1350	3100	5·4	10·33	22	1·55	401	22	1·55	401	6	0·08	295	1·66
G12-1	23·6	300	200	250	1350	3100	5·4	10·33	25	3·04	407	25	3·04	407	6	0·08	295	1·52
G13-1	23·6	400	200	350	1350	3100	3·86	7·75	25	1·45	406	25	1·45	406	6	0·06	295	2·11
G14-1	23·6	350	200	300	1350	3100	4·5	8·86	25	1·69	406	25	1·69	406	6	0·07	295	1·96
G15-1	23·6	400	200	350	1350	3100	3·86	7·75	25	1·11	406	25	1·11	406	6	0·06	295	3·58
G16-1	23·6	370	200	320	1350	3100	4·22	8·38	25	1·58	406	25	1·58	406	6	0·06	295	2·16

n/a= not applicable

Continued

Appendix 2 Impact response characteristics

Beam ID	Mass of impactor: kg	Height of impactor: m	Impact velocity: m/s	Input kinetic energy: kJ	Maximum impact force: kN	Maximum reaction force: kN	Maximum displacement: mm	Failure mode
Kishi *et al*. (2001)								
A19	200	n/p	1·00	0·1	n/p	41·9	n/p	n/p
A22	200	n/p	1·00	0·1	n/p	n/p	n/p	n/p
B10	200	n/p	1·00	0·1	21·9	29·2	0·45	n/p
B13	200	n/p	1·00	0·1	n/p	n/p	n/p	n/p
B19	200	n/p	1·00	0·1	n/p	46·9	n/p	n/p
C10	200	n/p	1·00	0·1	n/p	n/p	n/p	n/p
C13	200	n/p	1·00	0·1	n/p	21·6	n/p	n/p
C19	200	n/p	1·00	0·1	n/p	n/p	n/p	n/p
Kishi *et al*. (2002)								
A24	300	0·05	1·00	0·15	90·9	93·5	1·1	n/p
	300	0·46	3·00	1·35	144·4	113·4	10·6	n/p
	300	0·82	4·00	2·4	183·5	162·9	15·1	n/p
	300	1·27	5·00	3·75	194·3	161·2	29·6	n/p
	300	1·84	6·00	5·4	197·3	161·4	53·6	n/p
A36	300	0·05	1·00	0·15	62·2	60·3	1·6	Flexure
	300	0·46	3·00	1·35	124·2	121·5	11·3	Diagonal tension (one side)
	300	0·82	4·00	2·4	117·9	125·6	28·8	Diagonal tension (both sides)
	300	1·27	5·00	3·75	142·2	105·1	70	Disintegration
A48	300	0·05	1·00	0·15	40·3	40·3	4	n/p
	300	0·46	3·00	1·35	90·1	90·1	13·7	n/p
	300	0·82	4·00	2·4	125	107·9	18·4	n/p
	300	1·27	5·00	3·75	141·6	104·6	145·8	n/p
B24	300	0·05	1·00	0·15	69·3	70·1	2·3	n/p
	300	0·2	2·00	0·6	101·3	95	6·6	n/p
	300	0·46	3·00	1·35	124·3	98·8	15·1	n/p
	300	0·82	4·00	2·4	125·7	94·5	17	n/p
	300	1·27	5·00	3·75	136·4	110·3	53·3	n/p
B36	300	0·05	1·00	0·15	44·9	43·1	2·9	Flexure
	300	0·46	3·00	1·35	87	71·5	17·1	Flexure
	300	0·82	4·00	2·4	104·7	72·2	27·1	Flexure–compression
	300	1·27	5·00	3·75	128·8	80·1	109·3	Diagonal tension (one side)

(continued on next page)

Beam ID	Mass of impactor: kg	Height of impactor: m	Impact velocity: m/s	Input kinetic energy: kJ	Maximum impact force: kN	Maximum reaction force: kN	Maximum displacement: mm	Failure mode
B48	300	0·05	1·00	0·15	39·4	31·6	4·5	n/p
	300	0·46	3·00	1·35	94·5	56·7	21·8	n/p
	300	0·82	4·00	2·4	111·7	86	36·5	n/p
	300	1·27	5·00	3·75	133	110·3	52·8	n/p
	300	1·84	6·00	5·4	148·4	114·5	135·1	n/p
Bhatti *et al.* (2009)								
A37	384	0·7	3·67	2·7	765	657	8·13	Diagonal cracks and shear plug from impactor point to bottom portion of beam
A46	384	1·08	4·58	4·2	900	732	10·13	More diagonal cracks, formation of shear plug and flexural cracks
A56	384	1·6	5·61	6·3	1007	938	13·13	Diagonal cracks and more pronounced shear plug
A65	384	2·15	6·52	8·5	1125	929	16	Shear plug and diagonal tension failure
A74	384	2·79	7·42	11	1250	1125	22	More diagonal cracks and shear plug
A84	384	3·6	8·40	14·1	1350	1088	24·38	Diagonal tension failure and spalling of concrete on top of the beam
B37	384	0·7	3·67	2·7	782	635	7·5	Diagonal cracks and flexural cracks
B46	384	1·08	4·58	4·2	900	816	11·25	More diagonal and flexural cracks
B65	384	2·15	6·52	8·5	1219	954	16	Diagonal cracks and formation of shear plug
B74	384	2·79	7·42	11	1350	1160	19·8	Width of diagonal crack in one side increases and spalling of concrete in impact zone starts
B84	384	3·6	8·40	14·1	1382	1214	24	One-sided diagonal cracks and number of cracks increases in impact zones

(continued on next page)

Beam ID	Mass of impactor: kg	Height of impactor: m	Impact velocity: m/s	Input kinetic energy: kJ	Maximum impact force: kN	Maximum reaction force: kN	Maximum displacement: mm	Failure mode
B93	384	4·41	9·30	17·3	1519	1160	28	More wide diagonal cracks on both sides, increased number of cracks and more spalling of concrete at the top surface
Fujikake *et al*. (2009)								
S1616	400	0·15	1·73	0·6	119	n/p	5·9	Flexure
	400	0·3	2·45	1·2	164	n/p	11·01	Flexure
	400	0·6	3·46	2·4	245	n/p	20·11	Flexure
	400	1·2	4·85	4·7	314	n/p	36·17	Flexure
S1322	400	0·3	2·45	1·2	177	n/p	7·79	Flexure
	400	0·6	3·46	2·4	262·6	n/p	11·44	Flexure
	400	1·2	4·85	4·7	303·3	n/p	23·45	Local failure with heavily crushed concrete at impact point
	400	2·4	6·86	9·4	314·8	n/p	27·03	Same as above
S2222	400	0·3	2·45	1·2	204·2	n/p	6·99	Flexure
	400	0·6	3·46	2·4	262·7	n/p	11·04	Flexure
	400	1·2	4·85	4·7	309·9	n/p	21·42	Local failure with heavily crushed concrete at impact point
	400	2·4	6·86	9·4	353·2	n/p	31·82	Same as above
Chen and May (2009)								
A1	98·7	2·72	7·30	2·63	n/p	n/p	n/p	Flexural failure and no spalling of impact zone
	98·7	2·72	7·30	2·63	223	n/p	n/p	Same as above
	98·7	2·72	7·30	2·63	234	n/p	n/p	Same as above
	98·7	2·72	7·30	2·63	233	n/p	n/p	Same as above
	98·7	2·72	7·30	2·63	n/p	n/p	n/p	Same as above
	98·7	2·72	7·30	2·63	229	n/p	n/p	Same as above
A1	98·7	2·72	7·30	2·63	128	n/p	n/p	Same as above
A2	98·7	2·72	7·30	2·63	214	n/p	n/p	Same as above
	98·7	2·72	7·30	2·63	230	n/p	n/p	Same as above
A3	98·7	2·72	7·30	2·63	194	n/p	n/p	Same as above

(continued on next page)

Beam ID	Mass of impactor: kg	Height of impactor: m	Impact velocity: m/s	Input kinetic energy: kJ	Maximum impact force: kN	Maximum reaction force: kN	Maximum displacement: mm	Failure mode
B1	98·7	2·72	7·30	2·63	n/p	n/p	n/p	High yielding or rupture of tension steel, spalling of impact zone
	98·7	2·72	7·30	2·63	161	n/p	n/p	Same as above
B1	98·7	2·72	7·30	2·63	183	n/p	n/p	Same as above
B2	98·7	2·72	7·30	2·63	169	n/p	n/p	Same as above
	98·7	2·72	7·30	2·63	171	n/p	n/p	High yielding or rupture of tension steel, spalling of impact zone, also scabbing and spalling
B3	98·7	2·72	7·30	2·63	654	n/p	n/p	Scabbing and spalling
B3	98·7	2·72	7·30	2·63	215	n/p	n/p	Scabbing and spalling
B4	98·7	2·72	7·30	2·63	241	n/p	n/p	Scabbing and spalling
Saatci and Vecchio (2009)								
SS0a	211	3·26	8·00	6·75	n/p	305	9·3	Several diagonal cracks on both sides but one side slightly wider 0·5 mm in width
SS0b	600	3·26	8·00	19·18	n/p	n/p	n/p	Extensive damage: massive concrete spalling at top and bottom, longitudinal reinforcements exposed and bent, bond failure at support
SS1a	211	3·26	8·00	6·75	n/p	356	12·1	Diagonal cracks on both sides and shear plug with 0·25 mm wide cracks under impact point
SS1b	600	3·26	8·00	19·18	n/p	625	39·5	Diagonal cracks up to 5 mm wide and 0·9 mm wide vertical cracks at midspan
SS2a	211	3·26	8·00	6·75	n/p	327	10	Several minor cracks and 0·2 mm wide diagonal crack
SS2b	600	3·26	8·00	19·18	n/p	592	37·9	Several diagonal cracks, one 1·8 mm wide and vertical cracks (1·3 mm) in midspan
SS3a	211	3·26	8·00	6·75	n/p	431	10·7	One-sided 0·15 mm wide diagonal crack with approx. 45° inclination

(continued on next page)

Beam ID	Mass of impactor: kg	Height of impactor: m	Impact velocity: m/s	Input kinetic energy: kJ	Maximum impact force: kN	Maximum reaction force: kN	Maximum displacement: mm	Failure mode
SS3b	600	3·26	8·00	19·18	n/p	682	35·3	Several diagonal cracks (0·4 mm) and vertical cracks (1 mm) in midspan
Tachibana *et al*. (2010)								
A1	300	n/p	5·00	3·75	434	n/p	24·1	n/p
A2-1	150	n/p	3·46	0·9	320·5	n/p	13·6	n/p
A2-2	300	n/p	2·45	0·9	293·4	n/p	25·4	n/p
A2-3	450	n/p	2·00	0·9	245·3	n/p	37	n/p
A2-4	150	n/p	4·90	1·8	453·4	n/p	16·3	n/p
A2-8	300	n/p	4·24	2·7	513·3	n/p	33·3	n/p
A2-9	450	n/p	3·46	2·7	444·6	n/p	48·4	n/p
A2-10	300	n/p	1·00	0·15	65·4	n/p	4·5	n/p
A2-11	300	n/p	2·00	0·6	253·2	n/p	12·6	n/p
A2-12	300	n/p	3·00	1·35	426·2	n/p	26·9	n/p
A2-13	300	n/p	4·00	2·4	489·3	n/p	41·4	n/p
A2-14	300	n/p	5·00	3·75	466·2	n/p	58·3	n/p
A4	300	n/p	5·00	3·75	451·5	n/p	114·9	n/p
B	300	n/p	5·00	3·75	667·1	n/p	77	n/p
C	300	n/p	5·00	3·75	650·3	n/p	42·4	n/p
D	300	n/p	5·00	3·75	638·7	n/p	94	n/p
E	300	n/p	5·00	3·75	742·2	n/p	29·1	n/p
F	300	n/p	5·00	3·75	663·5	n/p	43·9	n/p
Kishi and Mikami (2012)								
G1-1	300	2·5	7·00	7·35	1495·6	278·5	64·3	n/p
G1-1S	300	2·5	7·00	7·35	1600·6	287·6	58	n/p
G2-1	300	0·82	4·01	2·41	510·2	95·3	28·3	n/p
G2-2	300	1·28	5·01	3·77	779·3	92·9	44	n/p
G2-3	300	1·84	6·01	5·41	853·5	149·6	57	n/p
G2L-1	400	0·82	4·01	3·22	446·6	99	44·2	Flexural cracks from lower and upper fibre, diagonal shear cracks around midspan area
G3-1	300	0·82	4·01	2·41	1208·5	80·6	36·7	n/p
G3-2	300	1·28	5·01	3·77	1469·5	126·4	52	n/p
G3-3	300	1·84	6·01	5·41	1038·6	169	70·6	n/p
G4-1	300	0·82	4·01	2·41	800·3	122·5	39·7	n/p
G4-2	300	1·28	5·01	3·77	985·8	153·6	56·1	n/p

(continued on next page)

Beam ID	Mass of impactor: kg	Height of impactor: m	Impact velocity: m/s	Input kinetic energy: kJ	Maximum impact force: kN	Maximum reaction force: kN	Maximum displacement: mm	Failure mode
G5-1	400	1·84	6·01	7·22	1313·2	317·2	63·5	Flexural cracks from lower and upper fibre, diagonal shear cracks around midspan area
G5-2	400	2·5	7·00	9·81	1557·1	363·3	83·4	Same as above
G6-1	300	1·28	5·01	3·77	1335·9	268·4	26·4	n/p
G7-1	300	1·28	5·01	3·77	1242·8	181·1	45·8	n/p
G7-2	300	1·84	6·01	5·41	1588·3	192·8	60·9	n/p
G8-1	300	1·84	6·01	5·41	1192·1	277·5	36·5	n/p
G9-1	300	1·28	5·01	3·77	931·2	208·5	43·2	n/p
G9-2	300	1·84	6·01	5·41	1102·7	248·2	57·9	n/p
G10-1	300	0·82	4·01	2·41	750·7	173·3	33·7	Flexural cracks from lower and upper fibre, diagonal shear cracks around midspan area
G10-2	300	1·28	5·01	3·77	922·3	183·6	49·5	Same as above
G10-3	300	1·84	6·01	5·41	1016·9	188·3	67·8	Same as above
G10-4	300	2·5	7·00	7·35	1042·3	172·7	83·9	Same as above
G11-1	500	0·5	3·13	2·45	702·8	230·8	20·5	n/p
G11-2	500	0·9	4·20	4·41	971	380	33·2	n/p
G11-3	500	1·3	5·05	6·37	1461·5	372·4	43·1	n/p
G11-4	500	1·7	5·78	8·34	1877·8	379	55·5	n/p
G11-5	500	2·1	6·42	10·3	1764·8	379·3	67·2	n/p
G11-6	500	2·5	7·00	12·26	1906·6	408·1	83·4	n/p
G12-1	500	3	7·67	14·71	1675	397·5	85·4	n/p
G13-1	500	3	7·67	14·71	2150	598·7	60·6	n/p
G14-1	500	3	7·67	14·71	2258·1	539·6	63·7	n/p
G15-1	500	3	7·67	14·71	2062·9	630·4	40·5	n/p
G16-1	500	3	7·67	14·71	2022·6	567·7	52·9	n/p

n/p = not provided

Continued

REFERENCES

Adhikary SD, Li B and Fujikake K (2015) Low velocity impact response of reinforced concrete beams: experimental and numerical investigation. *International Journal of Protective Structures* **6(1)**: 81–111.

Bhatti AQ, Kishi N, Mikani H and Ando T (2009) Elasto-plastic impact analysis of shear-failure-type RC beams with shear reinforcements. *Materials and Design* **30**: 502–510.

CEB (Comite Euro-International du Beton) (1993) *CEB-FIP Model Code 1990*. Redwood Books, Trowbridge, UK.

CEB (2010) *CEB-FIP Model Code 2010*, vol. I. Comite Euro-International du Beton, Lausanne, Switzerland.

Chen Y and May IM (2009) Reinforced concrete members under drop-weight impacts. *Proceedings of the Institution of Civil Engineers – Structures and Buildings* **162(1)**: 45–56, http://dx.doi.org/10.1680/stbu.2009.162.1.45.

Cotsovos DM and Pavlovic MN (2008) Numerical investigation of concrete subjected to high rates of uniaxial tensile loading. *International Journal of Impact Engineering* **35(5)**: 319–335.

Fu HC, Erki MA and Seckin M (1991) Review of effects of loading rate on reinforced concrete. *Journal of Structural Engineering* **117(12)**: 3660–3679.

Fujikake K, Li B and Soeun S (2009) Impact response of reinforced concrete beam and its analytical evaluation. *Journal of Structural Engineering* **135(8)**: 938–950.

Grote DL, Park SW and Zhou M (2001) Dynamic behaviour of concrete at high strain rates and pressures: I experimental characterization. *International Journal of Impact Engineering* **25(9)**: 869–886.

Hughes G and Beeby AW (1982) Investigation of the effect of impact loading on concrete beam. *The Structural Engineer* **60B(3)**: 45–52.

Keenan WA and Feldman A (1960) *Behavior and Design of Deep Structural Members. Part 6. The Yield Strength of Intermediate Grade Reinforcing Bars under Rapid Loading*. University of Illinois, Urbana, IL, USA, Report to Research Directorate, Air Force Special Weapons Centre, Kirtland Air Force Base, New Mexico, Structural Research Series 197, Technical report ASFWC-TR-59-72.

Kim DJ, Sirijaroonchai K, El-Tawil SE and Naaman A (2010) Numerical simulation of the split Hopkinson pressure bar test technique for concrete under compression. *International Journal of Impact Engineering* **37(2)**: 141–149.

Kishi N and Mikami H (2012) Empirical formulas for designing reinforced concrete beams under impact loading. *ACI Structural Journal* **109(4)**: 509–519.

Kishi N, Nakano O, Matsouka KG and Ando T (2001) Experimental study on ultimate strength of flexural-failure-type RC beams under impact loading. *Transactions of SMiRT 16, paper 1525, Washington, DC, USA*.

Kishi N, Mikami H, Matsuoka KG and Ando T (2002) Impact behavior of shear-failure type RC beams without shear reinforcement. *International Journal of Impact Engineering* **27(9)**: 955–968.

Li QM and Meng H (2003) About the dynamic strength enhancement of concrete-like material in a Split Hopkinson pressure bar test. *International Journal of Solid and Structures* **40(2)**: 343–360.

Lu YB and Li QM (2011) About the dynamic uniaxial tensile strength of concrete-like materials. *International Journal of Impact Engineering* **38(4)**: 171–180.

Malvar LJ (1998) Review of static and dynamic properties of steel reinforcing bars. *ACI Materials Journal* **95(5)**: 609–616.

Malvar LJ and Ross CA (1998) Review of strain rate effects for concrete in tension. *ACI Materials Journal* **95(6)**: 735–739.

Ozbolt J, Bosnjak J and Sola E (2013) Dynamic fracture of concrete compact tension specimen: Experimental and Numerical study. *International Journal of Solids and Structures* **50**: 4270–4278.

Ozbolt J, Sharma A and Reinhardt HW (2011) Dynamic fracture of concrete compact tension specimen. *International Journal of Solids and Structures* **48(10)**: 1534–1543.

Ross A, Tedesco JW and Kuennen ST (1995) Effect of strain rate on concrete strength. *ACI Materials Journal* **92(1)**: 37–47.

Ross A, Jerome DM, Tedesco JW and Hughes ML (1996) Moisture and strain rate effects on concrete strength. *ACI Materials Journal* **93(3)**: 293–300.

Rossi P, Van Mier JGM, Toutlemonde F, Le Maou F and Boulay C (1994) Effect of loading rate on strength of concrete subjected to uniaxial tension. *Material and Structures* **27(5)**: 260–264.

Saatci S and Vecchio F (2009) Effects of shear mechanisms on impact behaviour of reinforced concrete beams. *ACI Structural Journal* **106(1)**: 78–86.

Soroushian P and Choi K (1987) Steel mechanical properties at different strain rates. *Journal of Structural Engineering* **113(4)**: 663–672.

Soroushian P, Choi KB and Alhamad A (1986) Dynamic constitutive behavior of concrete. *ACI Journal* **83(2)**: 251–259.

Tachibana S, Masuya H and Nakamura S (2010) Performance based design of reinforced concrete beams under impact. *Natural Hazards and Earth System Sciences* **10(6)**: 1069–1078.

Tedesco JW and Ross CA (1998) Strain-rate-dependent constitutive equations for concrete. *ASME Journal of Pressure Vessel Technology* **120(4)**: 398–405.

Tedesco JW, Powell JC, Ross CA and Hughes ML (1997) A strain-rate dependent concrete material model for ADINA. *Computer and Structures* **64(5/6)**: 1053–1067.

Wakabayashi M, Nakamura T, Yoshida N, Iwai S and Watanabe Y (1980) Dynamic loading effects on the structural performance of concrete and steel materials and beams. *Proceedings of the 7th World Conference on Earthquake Engineering, Istanbul, Turkey*, pp. 271–278.

Xiao S, Li H and Monteiro PJM (2010) Influence of strain rates and load histories on the tensile damage behaviour of concrete. *Magazine of Concrete Research* **62(12)**: 887–894, http://dx.doi.org/10.1680/macr.2010.62.12.887.

Zhou XQ and Hao H (2008) Modeling of compressive behavior of concrete-like materials at high strain rate. *International Journal of Solid and Structures* **45(17)**: 4648–4661.

WHAT DO YOU THINK?

To discuss this paper, please submit up to 500 words to the editor at journals@ice.org.uk. Your contribution will be forwarded to the author(s) for a reply and, if considered appropriate by the editorial panel, will be published as a discussion in a future issue of the journal.